DOI: 10.1002/ejic.200600258

Synthesis, Crystal Structure, and Second-Order Nonlinear Optical Properties of Ruthenium(II) Complexes with Substituted Bipyridine and Phenylpyridine Ligands

Laurence Labat,[a] Jean-François Lamère,[a] Isabelle Sasaki,[a] Pascal G. Lacroix,*[a] Laure Vendier,[a] Inge Asselberghs,[b] Javier Pérez-Moreno,[b] and Koen Clays[b]

Keywords: Ligand design / Donor–acceptor systems / Ruthenium / Nonlinear optics / Density functional calculations

Two new ruthenium(II) complexes of formula $[Ru(bpy)_2(L^1)][PF_6]$ and $[Ru(bpy)_2(L^2)][PF_6]_2$ are reported. HL^1 is a (nitrophenyl)ethenyl-substituted phenylpyridine ligand, and L^2 is the bipyridine analogue of HL^1. The X-ray crystal structure of $[Ru(bpy)_2(L^1)][PF_6]$ has been solved, and the compound is found to crystallize in the monoclinic *C*2/*c* space group. The electronic spectrum of the cyclometalated derivative $[Ru(bpy)_2(L^1)][PF_6]$ exhibits a low-lying transition that is red-shifted from 454 to 546 nm relative to that of the parent bipyridine-based complex, which reveals an important charge-transfer character. To support this assumption, the nonlinear optical properties were investigated by the hyper-Rayleigh scattering technique and indicate a molecular static hyperpolarizability (β_0) equal to 230×10^{-30} cm^5 esu^{-1}.

Introduction

Molecules with π-conjugated electronic structures have been attracting considerable interest due to their potential nonlinear optical (NLO) properties and applications in optoelectronic and photonic devices.[1,2] While the first investigations were initially focused on purely organic systems,[3] the search for alternative organometallic and inorganic derivatives has gradually intensified in the last fifteen years.[4–6] Incorporation of metal atoms into π-conjugated systems introduces many new variables, such as diversity of oxidation states, intensely colored charge-transfers, additional magnetic capabilities, and a diversity of new topologies, which leads to NLO chromophores of much greater complexity than that of the first generation of "push-pull" organic molecules.[6]

For instance, ruthenium complexes have provided intriguing molecular materials with unusual electronic capabilities since the 1960s, in particular as mixed-valence $Ru^{II}Ru^{III}$ complexes.[7] In (pyridine)ruthenium(II) complexes, for example, the metal center is engaged in π-bonding with the organic ligating groups and can be involved in strongly allowed metal-to-ligand charge-transfer (MLCT), and hence provides various candidates for NLO applications. Indeed, ruthenium has led to the most investigated family of (pyridine)metal complexes in nonlinear optics.[8] The reasons for this interest are the possibility of designing various promising octupolar topologies,[9,10] and the observation of switchable NLO responses upon metal oxidation in some cases,[11] a possibility which could attract great interest in relation with the concept of molecular switches.[12,13]

In the last few years several cyclometalated counterparts of (polypyridine)ruthenium complexes have been prepared and their physical properties reported.[14–17] In fact, cyclometalated complexes have found widespread interest as species with promising properties in various research fields[15c] owing to the strong σ-donor ability of the cyclometalating ligand. Basically, replacement of a nitrogen donor by a formal carbanion donor drastically increases the electron density around the metal atom and the crystal-field strength.[14,15a] As a consequence, the d→π* back-donation is reinforced, which leads to a potential enhancement of the overall intramolecular charge transfer, a property which is highly desirable for the design of NLO chromophores. The enhancement of the donating capabilities of the ruthenium(II) center has been evidenced experimentally by the observation of intense charge-transfer properties in Ru^{II}/Ru^{III} complexes with bis(cyclometalating) ligands,[15b,18] and by a shift of the value of the Ru^{II}/Ru^{III} oxidation potential of about 900 mV upon replacement of one nitrogen atom by one carbon atom in tris(bipyridine)ruthenium(II)-like complexes.[14]

Recently, we have developed a new synthetic strategy aimed at providing an access to numerous phenylpyridine ligands substituted in *para* (R^1) and *meta* (R^2) positions with respect to the nitrogen atom (Scheme 1).[19] In the perspective of nonlinear optics, the presence of an acceptor (A) in the *meta* position is the most desirable to favor an intense

[a] Laboratoire de Chimie de Coordination du CNRS, 205 route de Narbonne, 31077 Toulouse, France
[b] Department of Chemistry, University of Leuven, Celestijnenlaan 200D, 3001 Leuven, Belgium

charge-transfer process from electron-rich metal–carbon moieties, as indicated in this scheme, and finally to provide a sizeable NLO response.

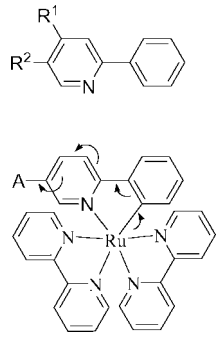

Scheme 1.

Following this idea, we report here our attempt to design a set of two (phenylpyridine and bipyridine)ruthenium complexes with potential MLCT capabilities. In the first section, their synthesis and characterizations will be presented. Then, the crystal structure of the cyclometalated complex will be discussed. Finally, the optical and nonlinear optical properties of both derivatives will be compared in relation to the enhanced "push-pull" character induced by the Ru–C linkage. The investigated molecules of formula $[Ru(bpy)_2(L^1)][PF_6]$ and $[Ru(bpy)_2(L^2)][PF_6]_2$ are shown in Scheme 2.

Results and Discussion

Synthesis and Characterization

Two methods for the synthesis of HL^1 and L^2, which contain the electron-withdrawing substituent NO_2, were envisioned: by condensing formylbipyridine or formyl(phenyl)pyridine with the appropriate phosphonate (method A) or by condensing the phosphonate **3a**,**b** derived from the bipyridine or the phenylpyridine with *p*-nitrobenzaldehyde (method B). Method B was chosen as the synthesis of 5-(bromomethyl)-2,2′-bipyridine (**2b**) from **1b**[20] has already been described[21] and was extended here to 5-methyl-2-phenylpyridine (**1a**). The first step involves the conversion of the methyl group to the corresponding bromomethyl group by treatment with *N*-bromosuccinimide (NBS) and azoisobutyronitrile (AIBN). The bromomethyl derivatives **2a**,**b** were then converted into the phosphonate derivatives **3a**,**b**.[22] The final step was the Wadsworth–Emmons reaction of compounds **3a**,**b** with the commercially available *p*-nitrobenzaldehyde, which leads to the styryl derivatives HL^1 and L^2 in 29% and 37% yields, respectively.[22] The double-bond linkages were confirmed to be (*E*) by ^1H NMR analysis based on the value of the $J_{CH=CH}$ coupling constant (ca. 16 Hz).

The syntheses of the two complexes are not similar. The tris(bipyridine) complex was obtained by the classical method, i.e., heating of 1 equiv. of $[Ru(bpy)_2]Cl_2$ with

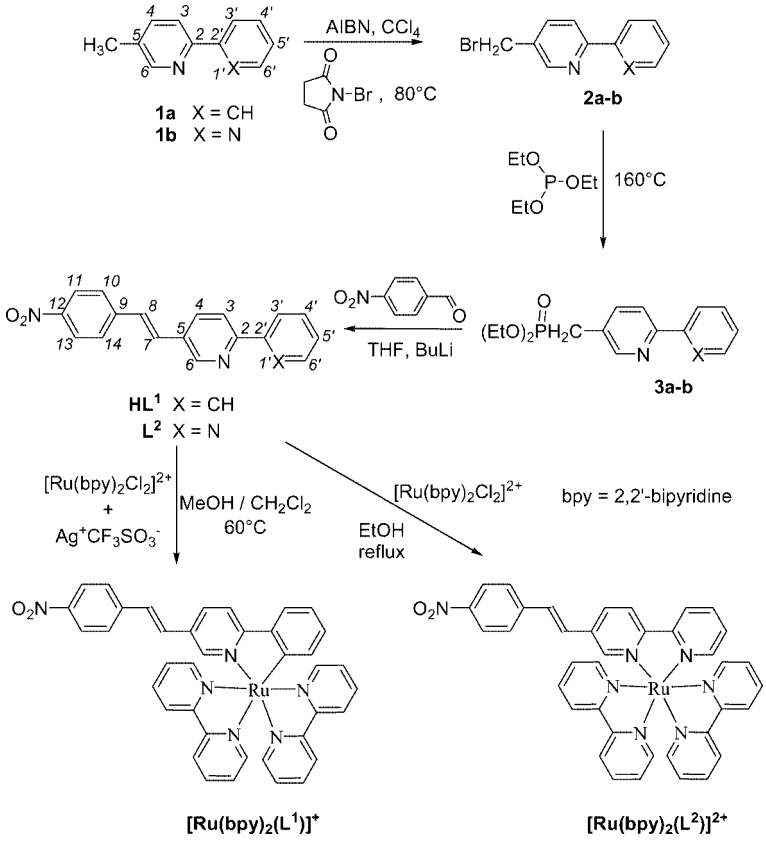

Scheme 2.

1 equiv. of L^2 in ethanol, whereas for the cyclometalated complex 1 equiv. of $[Ru(bpy)_2]Cl_2$ was treated with 5 equiv. of the phenylpyridine HL^1 in the presence of silver triflate.[19] The complexes were characterized by the usual methods. The labelling of the atoms is the one used for the X-ray structure. Characteristic peaks of cyclometalated compounds were observed in the NMR spectra of $[Ru(bpy)_2(L^1)][PF_6]$ and the peaks of the spectra were fully assigned.[14,23,24] Nevertheless, for complex $[Ru(bpy)_2(L^2)][PF_6]_2$, the unambiguous assignment of all the signals was not possible: since the electronic environments of numerous pyridine hydrogen atoms are nearly similar, their signals occur in a very narrow chemical-shift range.

Structural Data

The crystallographic data are summarized in the Experimental Section, and the X-ray molecular structure of $[Ru(bpy)_2(L^1)][PF_6]$ is presented in Figures 1 and 2. The compound crystallizes in the monoclinic *C*2/*c* space group ($Z = 8$). The asymmetric unit cell (Figure 1) is built up from one ruthenium complex, one PF_6^- anion, and one molecule of diethyl ether. In the crystal, $[Ru(bpy)_2(L^1)][PF_6]$ is organized in extended layers of complexes in the *bc* plane (Figure 2). The π-conjugated skeleton of the substituted phenylpyridine ligands lies parallel to the layers, the direction of highest polarizability (phenyl → NO_2) being roughly [001].

The ruthenium atom lies in a distorted octahedral environment. Metal–ligand bond lengths are presented in Table 1. Interestingly, and in contrast with previously reported X-ray data,[16] the Ru–C(1) distance of 2.033(4) Å is not significantly shortened with respect to the average Ru–N distance 2.036(4) Å observed for the bipyridine N(3), N(4) atoms. Nevertheless, a tendency for increased ruthenium–nitrogen bond lengths in the *trans* position with respect to the Ru–C bond is unambiguously seen [Ru–N(6) = 2.133(4) Å]. Along this line, the increase of this latter bond length is indeed the most noticeable geometrical change introduced in the coordination sphere of the metal atom by the presence of a carbon atom, in agreement with the

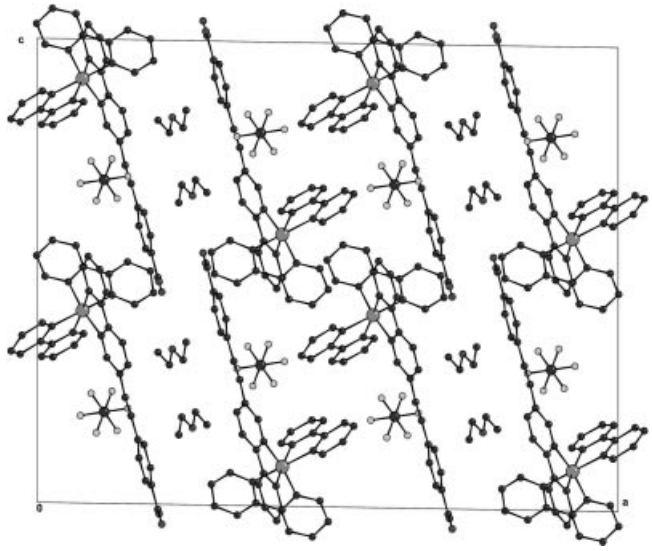

Figure 2. View of the crystal cell of $[Ru(bpy)_2(L^1)][PF_6]$ in the *ac* plane.

$[Ru(bpy)_2(nitrophenpy)]^+$ structure reported in the literature.[16] Another, more surprising, structural feature is the angle of 37.0(3)° observed between the phenyl group carrying the nitro substituent and the pyridine ring of the phenylpyridine ligand. This rotation suggests that the nitrophenyl group is not significantly involved in the charge-transfer process in the solid state. In order to verify whether the torsion arises from crystal packing or from intrinsic electronic effects, the gas-phase geometries of $[Ru(bpy)_2(L^1)][PF_6]$ and $[Ru(bpy)_2(L^2)][PF_6]_2$ were investigated within the framework of density functional theory (DFT).

The calculated coordination spheres are compared in Table 1. The tendency for slightly increases bond lengths obtained by DFT is observed here, as is the case in model Ru(phenpy) complexes (see Experimental Section). In the case of the bipyridine-based derivative, the six bond lengths are very similar, with an average value of 2.1175 Å. By contrast, the coordination sphere of the cyclometalated derivative exhibits the usual structural features of $[Ru(bpy)_2$-

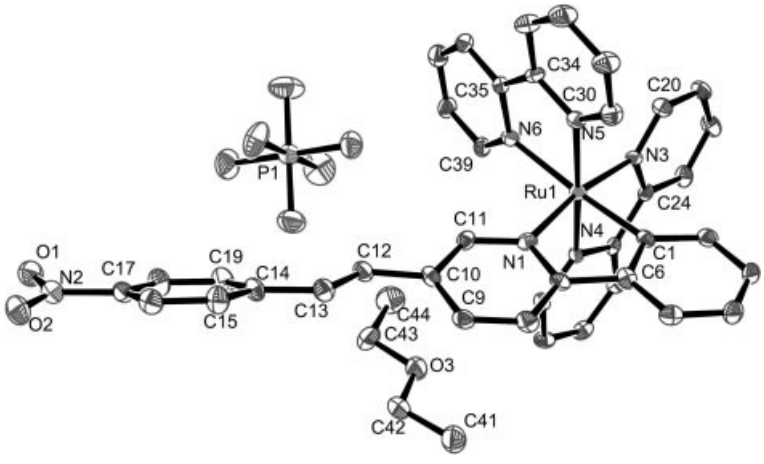

Figure 1. Asymmetric unit cell of $[Ru(bpy)_2(L^1)][PF_6]$. Hydrogen atoms are omitted for clarity.

Table 1. Ruthenium–ligand bond lengths [Å] in $[Ru(bpy)_2(L^1)][PF_6]$ and $[Ru(bpy)_2(L^2)][PF_6]_2$.

	$[Ru(bpy)_2(L^1)][PF_6]$		$[Ru(bpy)_2(L^2)][PF_6]_2$	
	X-ray	DFT	X-ray	DFT
Ru–C(1)	2.033(4)	2.049	n.a.	2.117
Ru–N(1)	2.072(3)	2.131	n.a.	2.120
Ru–N(3)	2.033(3)	2.088	n.a.	2.118
Ru–N(4)	2.039(4)	2.096	n.a.	2.116
Ru–N(5)	2.068(4)	2.124	n.a.	2.116
Ru–N(6)	2.133(4)	2.233	n.a.	2.118

$(phenpy)]^+$ complexes, namely a shortening of the Ru–C bond (2.049 Å) and elongation of the Ru–N bond (2.233 Å) *trans* to the Ru–C bond. Importantly, the angles between the nitrophenyl and pyridine rings are 4.4° and 3.1° for $[Ru(bpy)_2(L^1)]^+$ and $[Ru(bpy)_2(L^2)]^{2+}$, respectively. This result suggests that, to a large extent, the torsion angle of 37° observed in the crystal structure arises from a solid-state effect and is not an intrinsic electronic behavior of the chromophores.

Optical Properties

The UV/Vis spectra of $[Ru(bpy)_2(L^1)][PF_6]$ and $[Ru(bpy)_2(L^2)][PF_6]_2$ are shown in Figure 3. At first glance, both spectra are grossly similar and reveal three intense transitions located at 296 (65150), 370 (51850), and 546 (14500 $mol^{-1}\,L\,cm^{-1}$) nm for the cyclometalated complex, and at 288 (64850), 365 (44900), and 454 (12250 $mol^{-1}\,L\,cm^{-1}$) nm for the parent bipyridine-based derivative. It is interesting to note that the only significant difference in both spectra is a redshift of 92 nm (3711 cm^{-1}) observed for the low-lying transition depending on the presence of an Ru–N or Ru–C linkage. This considerable shift suggests that the low-energy transition is the main signature of the charge transfer arising between the ruthenium atom and the substituted bipyridine or phenylpyridine ligand.

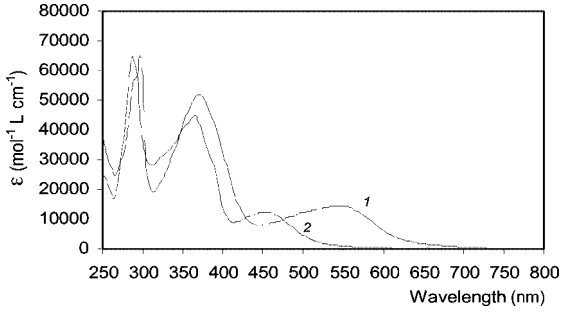

Figure 3. UV/Vis spectra of $[Ru(bpy)_2(L^1)][PF_6]$ (**1**) and $[Ru(bpy)_2(L^2)][PF_6]_2$ (**2**) recorded in acetonitrile.

In order to further analyze the nature of the electronic transitions of ruthenium complexes, the solvatochromic properties have been investigated. Solvatochromism is usually associated with a large dipole moment change upon electronic excitation, and is therefore an interesting probe of large charge-transfer capabilities. The absorption maxima recorded in solvents of different polarities are gathered in Table 2 and presented in Figure 4, where the energy transitions are drawn vs. the Reichardt solvent parameter E_T^N.[25] A first comparison conducted on the two transitions of the cyclometalated complex, located at 370 and 546 nm, confirms that the low-lying transition exhibits the largest solvatochromic shift (slope equal to 499 in Figure 4b, vs. 414 in Figure 4a). This is consistent with the anticipation of an intense charge-transfer effect associated with the low-lying transition of these ruthenium complexes. In a second comparison, the low-energy transitions are compared for $[Ru(bpy)_2(L^1)][PF_6]$ (Figure 4b) and the bipyridine-based $[Ru(bpy)_2(L^2)][PF_6]_2$ (Figure 4c). A reduction of the slope to 369 in Figure 4c clearly shows that the solvatochromic shift (and hence the charge transfer properties) are limited in $[Ru(bpy)_2(L^2)][PF_6]_2$. All together, these experimental data confirm the initial intuition that cyclometalated derivatives are promising candidates for the design of molecules with enhanced charge-transfer capabilities.

Table 2.Absorption maxima (λ_{max} [nm]) of the lowest-energy optical transitions for $[Ru(bpy)_2(L^1)][PF_6]$ and $[Ru(bpy)_2(L^2)][PF_6]_2$ in solvents of different polarities.

Solvent	$E_T^{N[a]}$	$[Ru(bpy)_2(L^1)][PF_6]$		$[Ru(bpy)_2(L^2)][PF_6]_2$	
MeOH	0.765	369	547.0	361.5	453.0
EtOH	0.654	370.5	549.0	362.0	453.5
1-PrOH	0.617	370.5	550.0	362.0	453.5
2-PrOH	0.552	370	548.5	362.5	453.0
MeCN	0.472	372	550.0	365.0	454.0
CH_2Cl	0.321	371.5	553.5	362.0	456.0
CHCl3	0.259	372.5	555.5	365.5	456.5

[a] Reichardt parameter.

A theoretical support is provided from the calculated electronic spectra. Functionals specifically designed for TD-DFT calculations of electronic spectra (LB94, SOAP, GRAC) are not implemented in our version of Gaussian, therefore the spectra were calculated with ZINDO on the basis of the gas-phase DFT structures. The data are gathered in Table 3, where they are compared to the experimental values. There is an important blueshift in the computed wavelengths for both complexes. However, this seems to be a general tendency frequently observed in the calculated spectra of inorganic chromophores.[26] The fact that the magnitude of this shift is especially pronounced in the case of the low-energy transition of $[Ru(bpy)_2(L^1)][PF_6]$, which is assumed to arise from an intense metal–phenyl charge transfer, may be additionally related to an enhancement of the ruthenium–ligand distance within the DFT computation. Apart from these energy differences, a qualitative agreement between experiment and calculation is observed on two important points: (i) both complexes exhibit a very intense high-energy transition and a less intense one located at lower energy; (ii) while the high-energy transitions are grossly located at the same energy range in both derivatives, the low-lying transition is considerably red-shifted in the case of the cyclometalated compound.

To further understand the nature of the charge-transfer behavior, the low-lying transitions can be analyzed at the

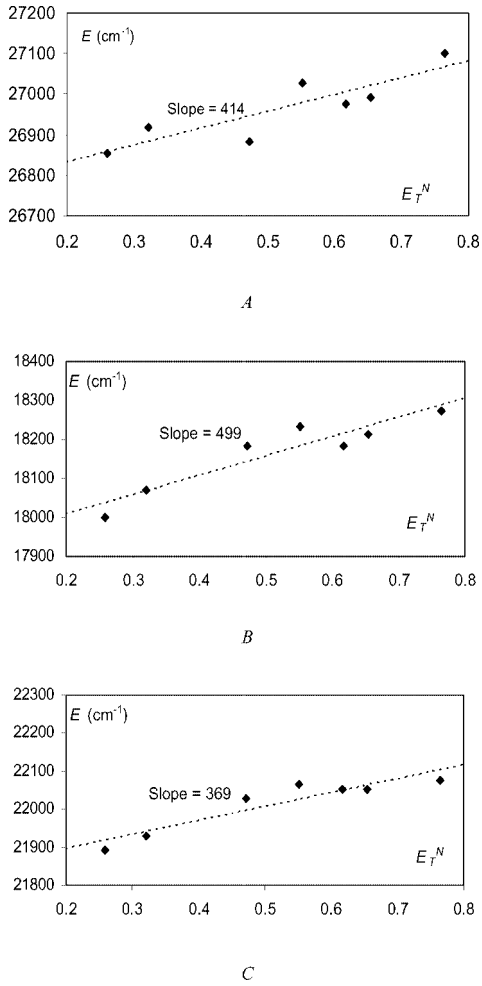

Figure 4. Absorption maxima [cm^{-1}] in solvents of different polarity (Reichardt constant E_T^N) for $[Ru(bpy)_2(L^1)][PF_6]$ [band at 370 (A) and 546 nm (B)] and for $[Ru(bpy)_2(L^2)][PF_6]_2$ [band at 454 nm (C)].

orbital level. In the case of $[Ru(bpy)_2(L^2)][PF_6]_2$, three dominant excitations contribute to the $1 \rightarrow 2$ transition (Table 3), which leads to 47% of the ground-state electron density in orbital 117. However, this orbital is located on the L^2 fragment only (98.1% of the electron density), which results in a ligand-to-ligand charge-transfer process. The contribution of the metal atom to $1 \rightarrow 2$ is weak and is provided by orbital 114 (70.0% centered on the ruthenium atom). In the case of $[Ru(bpy)_2(L^1)][PF_6]$, the dominant excitations involved in the $1 \rightarrow 7$ transition lead to the same 47% of ground-state electron density in orbital 117. However, and in striking contrast with $[Ru(bpy)_2(L^2)][PF_6]_2$, the electron density in orbital 117 is shared between L^1 (61.5%) and the ruthenium atom (31.8%). An additional donating contribution of the ruthenium atom is provided by orbital 115 (70.0% ruthenium-based). These differences lead to a significant enhancement of the donating character of the ruthenium atom in $[Ru(bpy)_2(L^1)][PF_6]$. The overall charge-transfer behavior associated with the $1 \rightarrow 7$ transition is shown in Figure 5, which clearly indicates that the ruthenium–phenyl fragment is deeply involved as the donating moiety of the chromophore.

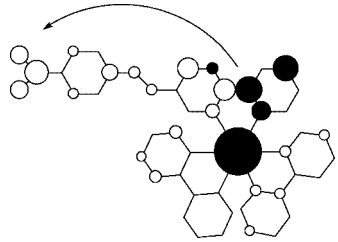

Figure 5. Charge transfer associated with the low-lying electronic transition of $[Ru(bpy)_2(L^1)][PF_6]$. White (black) contributions are indicative of increase (decrease) of electron density occurring upon electron transition.

Additional experimental evidence revealing the enhancement of the electron density around the metal center is provided by the electrochemical studies of the Ru^{II}/Ru^{III} oxidation process. Single-electron waves are observed in both complexes, leading to $E^{1/2}$ values equal to 0.49 and 1.30 V for $[Ru(bpy)_2(L^1)][PF_6]$ and $[Ru(bpy)_2(L^2)][PF_6]_2$, respectively. The effect of cyclometalation on the stability of the Ru^{III} state is illustrated by a cathodic shift of about 810 mV. This behavior demonstrates the strong σ-donating character of the anionic ligand, and the enhancement of the donating ability upon replacement of a nitrogen atom by a carbon atom, in the coordination sphere of the ruthenium atom.[19]

Nonlinear Optical Properties

Before describing the NLO response of $[Ru(bpy)_2(L^1)][PF_6]$ and $[Ru(bpy)_2(L^2)][PF_6]_2$, it is important to emphasize that the values are not overestimated by multiphoton fluorescence. This is experimentally verified by performing femtosecond hyper-Rayleigh scattering (HRS) ex-

Table 3. Experimental and ZINDO calculated spectra for $[Ru(bpy)_2(L^1)][PF_6]$ and $[Ru(bpy)_2(L^2)][PF_6]_2$.

Compound	UV/Vis spectra		ZINDO data		Assignment	Composition of CI expansion of the low-lying transitions[a]	Orbitals (% electron density on Ru^{II})
	λ [nm]	ε [$mol^{-1}Lcm^{-1}$]	λ [nm]	*f*			
$[Ru(bpy)_2(L^1)][PF_6]$	546	14500	412	0.43	$1 \rightarrow 7$	0.529 $\chi_{117\rightarrow123}$ – 0.436 $\chi_{117\rightarrow120}$ + 0.371 $\chi_{115\rightarrow119}$	119 (6.1%), 120 (0.3%), 123 (0.9%), 115 (70.0%), 117 (31.8%)
	370	51900	344	0.72	$1 \rightarrow 11$		
$[Ru(bpy)_2(L^2)][PF_6]_2$	454	12300	397	0.42	$1 \rightarrow 2$	0.529 $\chi_{117\rightarrow118}$ – 0.454 $\chi_{114\rightarrow118}$ – 0.434 $\chi_{117\rightarrow119}$	118 (0.2%), 119 (4.2%), 114 (70.0%), 117 (1.6%)
	364	44900	358	0.87	$1 \rightarrow 10$		

[a] Orbital 117 is the HOMO and orbital 118 the LUMO in both compounds.

periments as a function of modulation frequency.[27] The finite lifetime associated with any fluorescence results in a demodulation (reduction of amplitude) for higher frequencies.[28] As exemplified in Figure 6, no such demodulation is observed in the case of $[Ru(bpy)_2(L^1)][PF_6]$, thus implying that the HRS signal is not comprised of any multiphoton fluorescence contribution.[29]

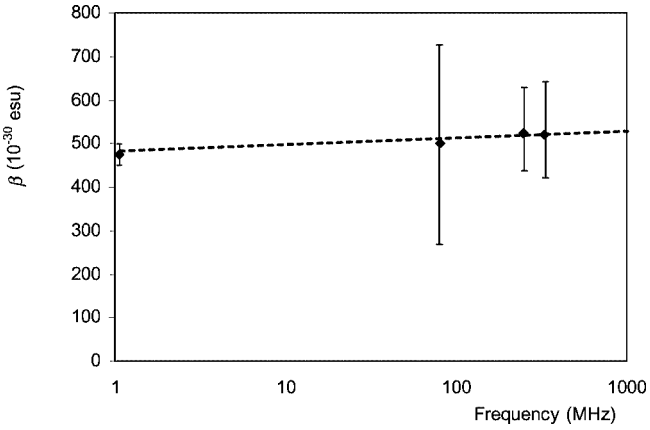

Figure 6. Experimental β values as a function of modulation frequency for $[Ru(bpy)_2(L^1)][PF_6]$, showing the frequency-independent response of the multiphoton-fluorescence-free HRS signal.

The HRS data are gathered in Table 4 for both derivatives. In the case of $[Ru(bpy)_2(L^2)][PF_6]_2$, the detected signal falls within the limit of the uncertainty of the present HRS setup; therefore the hyperpolarizability was not determined with full accuracy and the reported data are the upper β limit only. It must be pointed out that, as the second harmonic (400 nm) is close to the charge-transfer band located at 546 and 454 nm for $[Ru(bpy)_2(L^1)][PF_6]$ and $[Ru(bpy)_2(L^2)][PF_6]_2$, respectively, the experimental β values are necessarily overestimated by resonance. Therefore, the parameter to take into account as the intrinsic hyperpolarizability (independent of the laser frequency) is β_0 (vide infra). An examination of Table 4 reveals a significant enhancement of the NLO response in the cyclometalated derivative, with an intrinsic hyperpolarizability equal to 230×10^{-30} cm^5 esu^{-1}.

Table 4. Experimental hyperpolarizabilities [10^{-30} cm^5 esu^{-1}] for the ruthenium complexes, recorded using the hyper-Rayleigh scattering method at 800 nm (β) and at zero frequency (β_0).

	β	β_0
$[Ru(bpy)_2(L^1)][PF_6]$	500	230 (±50)
$[Ru(bpy)_2(L^2)][PF_6]_2$	< 200	< 40

Conclusions

Two related ruthenium(II) complexes have been investigated to compare their MLCT capabilities and hence the hyperpolarizabilities of metal–phenylpyridine- vs. metal–bipyridine-based chromophores. We have reported on a set of computational, spectroscopic, electrochemical, and nonlinear optical measurements which all prove that a strongly enhanced MLCT behavior takes place in a cyclometalated derivative with respect to the parent metal–bipyridine molecule. The last few years have witnessed a growing interest in (pyridine)ruthenium(II) complexes in relation with the concept of NLO switching obtained by a redox effect.[11] It therefore seems promising to design such cyclometalated ruthenium chromophores that exhibit large NLO responses in addition to reversible and accessible redox properties. Along these lines, these complexes could undoubtedly attract potential interest from the perspective of materials science.

Experimental Section

Starting Materials and Equipment: Reagents and solvents are commercially available and were used as received. **1a**,[19] **1b**,[20] and $[Ru(bpy)_2Cl_2]$[30] were prepared according to literature procedures. ^{1}H and ^{13}C NMR spectra were recorded at 298 K with a Bruker AM 250 spectrometer (250 MHz for ^{1}H NMR and 62.9 MHz for ^{13}C) or a Bruker Avance 500 spectrometer for 2D NMR. The atom labelling used for the assignment is given in Scheme 2. DCI and EI mass spectra were obtained with a Thermo Finnigan TSQ 7000 and FAB mass spectra were recorded with a quadrupolar Nermag R 10-10 instrument using an NBA matrix. UV/Vis spectra were recorded with a Hewlett Packard 8452A spectrophotometer. Elemental analyses were performed by the "Service de Microanalyses du Laboratoire de Chimie de Coordination" (Toulouse) with a Perkin–Elmer 2400 Serie II instrument. Cyclic voltammetry data were recorded with an Autolab PGSTAT 100 potentiostat, in acetonitrile using a Pt disk (1 mm diameter) as the working electrode, a Pt gauze as the auxiliary electrode, and SCE as the reference electrode. nBu$_4$NPF$_6$ (0.1 M) was used as the supporting electrolyte (purum electrochemical grade Fluka, purified by sublimation). All voltammetric experiments were performed at ambient temperature in a home-made, airtight three-electrode cell connected to a vacuum/argon line. The solutions used for the electrochemical studies were typically 10^{-3} M in ruthenium complex. Prior to measurements, the solutions were deoxygenated by bubbling with argon gas for 15 min and the working electrode was polished with a polishing machine (Presi P230); during experiments, a stream of argon was passed over the solution.

5-(Bromomethyl)-2-phenylpyridine (2a): 5-Methyl-2-phenylpyridine (**1a**; 2.11 g, 12.5 mmol), NBS (2.22 g, 12.9 mmol), and AIBN (36 mg) were refluxed in dry CCl_4 (58 mL) for 2 h. After cooling, the suspension was filtered. The solvent was removed in vacuo and n-hexane (30 mL) was added to the remaining paste. The mixture was stirred in an ice bath for 1 h, whereupon a white fleecy precipitate appeared. This was filtered off to yield the pure product (837 mg, 27%). ^{1}H NMR ($CDCl_3$): δ = 8.68 (s, 1 H), 7.97 (m, 2 H), 7.75 (m, 2 H), 7.45 (m, 3 H), 4.52 (s, 2 H) ppm. $C_{12}H_{10}BrN$ (248.1) + 0.25 H_2O: calcd. C 57.05, H 4.19, N 5.54; found C 56.81, H 3.95, N 5.57. DCI MS (NH_3): m/z (%) = 248.1 (33), 250.1 (34) $[MH]^+$.

5-(Bromomethyl)-2,2′-bipyridine (2b): Same procedure as for the synthesis of **2a**, starting from 5-methyl-2,2′-bipyridine (**1b**). Yield: 68%. The ^{1}H NMR spectrum is identical to those of previous reports.[31,32]

Diethyl (2-Phenylpyridin-5-yl)methylphosphonate (3a): Under nitrogen, **2a** (1.01 g, 4 mmol) was dissolved in triethyl phosphite (7 mL) and the mixture was refluxed for 1 d. After cooling, the brown oil was purified by two successive chromatographic separations on alumina (99% CH_2Cl_2/1% CH_3OH). Yellow oil (1.31 g, 87%). The

compound was used in the next step without further purification (triethyl phosphite could not be totally eliminated). ^{1}H NMR ($CDCl_3$): δ = 8.55 (s, 1 H), 7.95 (m, 2 H), 7.70 (m, 2 H), 7.42 (m, 3 H), 4.05 (m, 4 H), 3.14 (d, $J_{H,P}$ = 21.6 Hz, 2 H), 1.26 (t, J = 7.2 Hz, 6 H) ppm.

Diethyl (2,2′-Bipyridin-5-yl)methylphosphonate (3b): Same procedure as for the synthesis of **3a**, starting from **2b** and using 98% CH_2Cl_2/2% CH_3OH as eluent for the two chromatographic separations. Some traces of triethyl phosphite remained and the compound was used without any further purification (Yield: 76%). ^{1}H NMR ($CDCl_3$): δ = 8.66 (d, J = 4.2 Hz, 1 H), 8.56 (s, 1 H), 8.36 (d, J = 3.6 Hz, 1 H), 8.33 (d, J = 3.8 Hz, 1 H), 7.80 (m, 2 H), 7.28 (m, 1 H), 4.08 (q, J = 7 Hz, 4 H), 3.18 (d, $J_{H,P}$ = 22 Hz, 2 H), 1.35 (t, J = 6.8 Hz, 6 H) ppm.

5-(*p*-Nitrostyryl)-2-phenylpyridine (HL^1): In a Schlenk flask, **3a** (348 mg, 1.14 mmol) was dissolved in THF (21 mL) and cooled in an ice bath. *n*-Butyllithium (1.6 M in hexane; 0.72 mL, 1.15 mmol) was added dropwise and the solution was stirred at room temperature for 1 h. A THF solution (6 mL) of *p*-nitrobenzaldehyde (174 mg, 1.15 mmol) was then added slowly and the color changed from yellow to brown. The mixture was refluxed for 3 h. After cooling to room temperature, the mixture was hydrolyzed with water (10 mL). The precipitate was filtered off, washed with diethyl ether, and purified by column chromatography on alumina (80% CH_2Cl_2/20% *n*-pentane). The product was recovered as a lemon-yellow powder (200 mg, 37% yield). ^{1}H NMR ($CDCl_3$): δ = 8.86 (d, J = 2.1 Hz, 1 H, H6), 8.27 (d, J = 8.8 Hz, 2 H, H11, H13), 8.07 (dd, J = 8.7 and 1.4 Hz, 2 H, H2′, H6′), 7.98 (dd, J = 8.3 and 2.3 Hz, 1 H, H4), 7.81 (d, J = 8.3 Hz, 1 H, H3), 7.70 (d, J = 8.8 Hz, 2 H, H10, H14), 7.53 (dd, J = 7.6 and 7.1 Hz, 2 H, H3′, H5′), 7.47 (t, J = 7.3 Hz, 1 H, H4′), 7.31 (d, J = 16.3 Hz, 1 H, H7), 7.26 (d, J = 16.3 Hz, 1 H, H8) ppm. ^{13}C NMR ($CDCl_3$): δ = 155.22 (C2), 148.96 (C6), 147.08 (C12), 143.18 (C9), 138.59 (C1′), 133.87 (C4), 130.36 (C5), 129.41 (C4′), 129.35 (C7), 128.91 (C5′), 127.89 (C8), 127.10 (C10, C14), 126.89 (C6′), 124.27 (C11, C13), 120.48 (C3) ppm. $C_{19}H_{14}N_2O_2$ (302.3): calcd. C 75.48, H 4.67, N 9.27; found C 75.14, H 4.59, N 9.12. DCI MS (NH_3): m/z = 303 $[MH]^+$.

5-(*p*-Nitrostyryl)-2,2′-bipyridine (L^2): According to the procedure described above for the synthesis of HL^1, **3b** yielded compound L^2 (29% yield) after purification by chromatography on alumina with 0.5% MeOH in CH_2Cl_2. ^{1}H NMR ($CDCl_3$): δ = 8.84 (d, J = 1.9 Hz, 1 H, H6), 8.73 (ddd, J = 4.7, 1.6 and 0.8 Hz, 1 H, H6′), 8.51 (d, J = 8.3 Hz, 1 H, H3), 8.47 (d, J = 8 Hz, 1 H, H3′), 8.29 (d, J = 8.9 Hz, 2 H, H11, H13), 8.06 (dd, J = 8.3 and 2.3 Hz, 1 H, H4), 7.88 (td, J = 7.8 and 1.6 Hz, 1 H, H4′), 7.71 (d, J = 8.8 Hz, 2 H, H10, H14), 7.37 (ddd, J = 5.9; 4.9 and 1 Hz, 1 H, H5′), 7.34 (d, J = 16.5 Hz, 1 H, H7), 7.30 (d, J = 15.5 Hz, 1 H, H8) ppm. ^{13}C NMR ($CDCl_3$): δ = 155.70 (C2), 155.32 (C2′), 149.15 (C6′), 148.56 (C6), 147.16 (C12), 143.07 (C9), 137.25 (C4′), 133.99 (C4), 131.99(C5) 129.27 (C7), 128.50 (C8), 127.18 (C10, C14), 124.28 (C11, C13), 124.05 (C5′), 121.36 (C3′), 121.22 (C3) ppm. $C_{18}H_{13}N_3O_2$ (303.3): calcd. C 71.28, H 4.32, N 13.85; found C 70.78, H 3.94, N 13.53. EI-MS: m/z = 303 $[M]^+$.

$[Ru(bpy)_2(L^1)][PF_6]$: $[Ru(bpy)_2Cl_2]$ (40 mg, 0.073 mmol) and AgOTf (41 mg, 0.16 mmol) were added to a hot solution of HL^1 (110 mg, 0.36 mmol) in MeOH/CH_2Cl_2 (1:1, 10 mL) and the mixture was heated at 60 °C for 1 h. After cooling, the AgCl precipitate was filtered through glass fiber. The filtrate was concentrated and the crude product was purified by chromatography on alumina using two eluents: 0.5% MeOH in CH_2Cl_2 to recover the unreacted excess of ligand, then 3% MeOH in CH_2Cl_2 to isolate a dark-violet complex. A second chromatographic purification of this complex was carried out on alumina (3% MeOH in CH_2Cl_2) to yield the pure complex (15 mg, 24%). ^{1}H NMR (CD_3COCD_3): δ = 8.78 (td, J = 8.2 and 1.1 Hz, 1 H, H36), 8.68 (ddd, J = 8.1, 1.1 and 0.6 Hz, 1 H, H33), 8.62 (ddd, J = 8.2, 1.3 and 0.8 Hz, 1 H, H23), 8.60 (ddd, J = 8.3, 1.2 and 0.8 Hz, 1 H, H26), 8.21 (d, J = 8.8 Hz, 2 H, H16, H18), 8.24–8.17 (m, 3 H, H11, H37, H9), 8.16 (ddd, J = 5.7, 1.5 and 0.7 Hz, 1 H, H30), 8.10 (ddd, J = 5.4, 1.5 and 0.8 Hz, 1 H, H39), 8.06 (ddd, J = 5.8, 1.4 and 0.8 Hz, 1 H, H29), 8.00–7.90 (m, 6 H, H22, H32, H8, H5, H27, H20), 7.71 (d, J = 8.9 Hz, 2 H, H15, H19), 7.64 (ddd, J = 7.6, 5.4 and 1.2 Hz, 1 H, H38), 7.42–7.38 (m, 3 H, H21, H31, H28), 7.29 (d, J = 16.4 Hz, 1 H, H13), 7.21 (d, J = 16.4 Hz, 1 H, H12), 6.92 (dt, J = 7.2 and 1.2 Hz, 1 H, H4), 6.85 (dt, J = 7.2 and 1.3 Hz, 1 H, H3), 6.52 (dd, J = 7.4 and 1 Hz, 1 H, H2) ppm. ^{13}C NMR (CD_3COCD_3): δ = 194.27 (C1), 167.39 (C7), 157.90 (C34), 157.09 (C24), 156.80 (C25), 155.34 (C35), 154.27 (C30), 150.56 (C29), 150.04 (C20) 149.95 (C8), 149.23 (C39), 147.10 (C17), 145.26 (C6), 143.34 (C14), 136.59 (C37), 135.37 (C2), 135.19 (C32), 134.04 (C22), 133.77 (C27), 132.22 (C9), 131.17 (C10), 128.62 (C3), 128.46 (C12), 127.98 (C13), 127.37 (C38), 127.27 (C15, C19), 126.57 (C21), 126.40 (C31), 126.27 (C28), 124.85 (C5), 123.97 (C16, C18), 123.63 (C33), 123.41 (C36), 123.09 (C26), 123.08 (C23), 120.95 (C4), 118.39 (C11) ppm. The metathesis was carried out as follows: the complex with the triflate counterion was dissolved in the minimum amount of methanol then a saturated aqueous solution of NH_4PF_6 was added until no more precipitation occurred. The precipitate was filtered off, rinsed with distilled water and dried under vacuum. $C_{39}H_{29}F_6N_6O_2PRu$ (859.7) + H_2O: calcd. C 52.41, H 3.50, N 9.40; found C 52.38, H 3.30, N 9.12. FAB-MS: m/z = 715 $[M-PF_6]^+$.

$[Ru(bpy)_2(L^2)][PF_6]_2$: L^2 (48 mg, 0.158 mmol) was dissolved in EtOH (25 mL) under N_2 and the mixture heated to reflux. $[Ru(bpy)_2Cl_2]$ (85 mg, 0.158 mmol) was then added and the mixture refluxed for 3 h. After cooling in an ice bath, addition of NH_4PF_6 (saturated solution in water) led to the precipitation of the complex. The orange precipitate was filtered off, rinsed with water and diethyl ether, and dried in vacuo (115 mg). The compound was obtained by two successive chromatographic purifications on alumina (CH_3CN) and finally crystallization from acetone, which yielded the pure, brick-red complex (80 mg, 50%).^{1}H NMR (CD_3COCD_3): δ = 8.88–8.82 (m, 6 H, H8, H5, H26, H23, H33, H36), 8.60 (dd, J = 8.5, 1.9 Hz, 1 H, H9), 8.30–8.06 (m, 7 H, H11, H4, H27, H25, H32, H37, H39), 8.24 (d, J = 9 Hz, 2 H, H16, H18), 8.11 (dd, J = 5.6, 7 Hz, 1 H, H2), 8.09–8.06 (m, 3 H, H29, H20, H30), 7.76 (d, J = 8.8 Hz, 2 H, H15, H19), 7.64–7.58 (m, 5 H, H3, H31, H38, H21, H28), 7.57 (d, J = 16.4 Hz, 1 H, H12), 7.21 (d, J = 16.5 Hz, 1 H, H13) ppm. ^{13}C NMR (CD_3COCD_3): δ = 157.33, 157.24, 157.21, 157.04, 156.30, 152.07 (C11), 151.92 and 151.83 and 151.75 (C2, C29, C20, C30), 151.05, 147.62, 142.51, 138.09, and 138.00 (C37, C32, C25, C27), 136.53, 133.84 (C9), 132.01 (C12), 127.93, 127.88, 127.86, 127.84 (C15, C19), 127.75, 127.04 (C13), 124.60, 124.50, 124.48, 124.44, 124.35, 124.04, 114.38 ppm. $C_{38}H_{29}F_{12}N_7O_2P_2Ru$ (1006.7): calcd. C 45.34, H 2.90, N 9.74; found C 45.19, H 2.77, N 9.49. FAB-MS: m/z = 862 $[M-PF_6]^+$, 717 $[M-2PF_6]^+$.

Crystallographic Studies: Single crystals of $[Ru(bpy)_2(L^1)][PF_6]$ suitable for X-ray structure determination were grown by slow diffusion of diethyl ether into a concentrated solution of the complex in acetonitrile. Data were collected at 180 K with a Stoe Imaging Diffraction System (IPDS) equipped with a graphite-monochromated Mo-K_α radiation source (λ = 0.71073 Å) and an Oxford Cryosystems Cryostream Cooler Device. Empirical absorption corrections were applied (T_{min} = 0.811, T_{max} = 0.963).[33] The structure was solved by direct methods using SIR92,[34] and refined by means of least-squares procedures on F^2 with the aid of the program

SHELXL97[35] included in the software package WinGX version 1.63.[36] Final unit-cell parameters were obtained by means of a least-squares refinement of a set of well-measured reflections. The atomic scattering factors were taken from the International Tables for X-ray Crystallography.[37] All non-hydrogen atoms were refined anisotropically, and in the last cycles of refinement a weighting scheme was used, where weights are calculated with the following formula: $w = 1/[\sigma^2(F_o^2) + (aP)^2 + bP]$ where $P = (F_o^2 + 2F_c^2)/3$. Further details are listed in Table 5. The drawing of the molecule was produced with the program ORTEP32[38] with 50% probability displacement ellipsoids for non-hydrogen atoms. CCDC-602439 contains the supplementary crystallographic data for this paper. These data can be obtained free of charge from The Cambridge Crystallographic Data Centre via www.ccdc.cam.ac.uk/data_request/cif.

Table 5. Crystal data for $[Ru(bpy)_2(L^1)][PF_6]$ (**1**).

Empirical formula	$C_{29}H_{29}N_6O_2Ru{\cdot}C_4H_{10}O{\cdot}PF_6$
Formula mass	933.84
Crystal size [mm]	$0.425 \times 0.125 \times 0.0625$
Crystal system	monoclinic
Space group	*C*2/*c*
a [Å]	32.661(7)
b [Å]	9.5543(19)
c [Å]	26.044(5)
β [°]	90.92(2)
V [Å^3]	8126(3)
$\rho_{calcd.}$ [g cm^{-3}]	1.527
T [K]	180
μ (Mo-K_α) [mm^{-1}]	0.501
Scan mode	φ
θ range [°]	$2.22 < \theta < 26.10$
Measured reflections	37036
Independent reflections	7614
Observed reflections	7614
No of parameters	543
H atoms	calculated
R_1	0.0403
wR_2	0.0491
$\Delta\rho_{max}$ [e Å^{-3}]	0.518
$\Delta\rho_{min}$ [e Å^{-3}]	–1.143

Theoretical Methods: Gas-phase geometries for cations $[Ru(bpy)_2(L^1)]^+$ and $[Ru(bpy)_2(L^2)]^{2+}$ were fully optimized using the Gaussian-03 program package[39] within the framework of DFT at the B3LYP/6-31G*/LANL2DZ(Ru) level.[40,41] The starting metrical parameters for the calculations were taken from the present crystal structure of $[Ru(bpy)_2(L^1)]^+$. In the absence of a crystal structure for $[Ru(bpy)_2(L^2)][PF_6]_2$, the starting model was built up from the previously reported structures of $[Ru(bpy)_3][PF_6]_2$,[42] and 4-hydroxy-4′-nitrobiphenyl.[43] Due to the large size of the molecule, time-consuming vibrational analyses were not performed on the ruthenium complexes. Nevertheless, we checked that the DFT approach provides an accurate description of the molecular geometry in the case of the few previously reported $[Ru(bpy)(phenpy)]^+$ complexes,[16,19] although with a tendency for slightly inflated coordination spheres in the DFT-computed structures. The all-valence INDO (intermediate neglect of differential overlap) method[44] was employed to calculate the electronic transitions in order to analyze the origin of the charge transfer at the atomic level. Calculations were performed using the INDO/1 Hamiltonian incorporated in the commercially available MSI software package ZINDO.[45] The monoexcited configuration interaction (MECI) approximation was employed to describe the excited states. The 100 lowest-energy transitions between the 10 highest occupied molecular orbitals and the 10 lowest unoccupied ones were chosen to undergo CI mixing.

NLO Measurements: The experimental β measurements were performed with the frequency-resolved femtosecond hyper-Rayleigh scattering (HRS)[46] technique at 800 nm. This setup was used as described before.[27] The samples were dissolved in acetonitrile and crystal violet (CV) dissolved in methanol was used as the reference ($\beta_{xxx} = 338 \times 10^{-30}$ cm^5 esu^{-1}).[27] A concentration series ws measured and the slopes of the linear fitting compared. The internal field-correction factor $[(n^2+2)/3]^3$, where *n* is the refractive index at the Na_D line, was applied to correct for the difference in solvent ($n_{MeOH} = 1.328$ and $n_{MeCN} = 1.343$). The compounds were analyzed as dipolar structures with $C_{\infty v}$ symmetry. To correct for the difference in symmetry between the dipolar compound and octupolar reference, the following appropriate correction factors were used:[46b,47]

$$\beta^2_{zzz,dipole} = \frac{slope_{dipole}}{slope_{octupole}} \times \frac{28}{9} \times \frac{\left[\left(n^2_{MeOH}+2\right)/3\right]^6}{\left[\left(n^2_{MeCN}+2\right)/3\right]^6} \times \beta^2_{xxx,octupole} \quad (1)$$

The determined apparent hyperpolarizability was found to be independent of the modulation frequency, and the fluorescence-free hyperpolarizability was calculated by averaging the obtained hyperpolarizabilities at different modulation frequencies. Due to the weakness of the 2ω light intensity in the HRS phenomenon, measurements have to be performed close to the resonance, which leads to an artificial enhancement of the NLO signal. In this case, the parameter of interest is the intrinsic hyperpolarizability $\beta_{(0)}$, which is independent of the laser frequency and can be estimated within a two-level model according to the following expressions:[48]

$$\beta_\omega = \frac{3e^2\hbar^2 f_{ge}(\Delta\mu)_{ge}}{2mE_{ge}^3} \times \frac{E_{ge}^4}{\left(E_{ge}^2 - (2\hbar\omega)^2\right)\left(E_{ge}^2 - (\hbar\omega)^2\right)} \quad (2)$$

$$\beta_{(0)} = \frac{3e^2\hbar^2 f_{ge}(\Delta\mu)_{ge}}{2mE_{ge}^3} \quad (3)$$

Acknowledgments

The authors thank Dr. A. Sournia-Saquet for electrochemical measurements, CALMIP (Calcul en Midi Pyrénées, Toulouse) for parallel computation facilities, and a Programme d'Action Intégrée (PAI-Tournesol) for financial support.

[1] H. S. Nalwa, S. Miyata, *Nonlinear Optics of Organic Molecules and Polymers*, CRC Press, Boca Raton, FL, **1997**.
[2] M. G. Papadopoulos, J. Leszczynski, A. J. Sadlej, *Nonlinear Optical Properties of Matter: From Molecules to Condensed Phases*, Kluwer, Dordrecht, **2005**.
[3] D. S. Chema, J. Zyss, *Nonlinear Optical Properties of Organic Molecules and Crystals*, Academic Press, Orlando, FL, **1987**.
[4] a) S. Di Bella, *Chem. Soc. Rev.* **2001**, *30*, 355; b) P. G. Lacroix, *Eur. J. Inorg. Chem.* **2001**, 339.
[5] B. J. Coe, in *Comprehensive Coordination Chemistry II* (Eds.: J. A. McCleverty, T. J. Meyer), Elsevier Pergamon, Oxford, UK, **2004**, vol. 9, pp. 621.
[6] N. J. Long, *Angew. Chem. Int. Ed. Engl.* **1995**, *34*, 21.

[7] a) H. Taube, *Angew. Chem. Int. Ed. Engl.* **1984**, *23*, 329; b) C. Creutz, *Prog. Inorg. Chem.* **1983**, *30*, 1.
[8] H. Le Bozec, T. Renouard, *Eur. J. Inorg. Chem.* **2000**, 229.
[9] For an introduction of octupolar topologies, see: J. Zyss, I. Ledoux, *Chem. Rev.* **1994**, *94*, 77.
[10] For a recent review of ruthenium in octupolar geometry, see: H. Le Bozec, *Acc. Chem. Res.* **2005**, *38*, 691.
[11] a) B. J. Coe, S. Houbrechts, I. Asselberghs, A. Persoons, *Angew. Chem. Int. Ed.* **1999**, *38*, 366; b) B. J. Coe, *Chem. Eur. J.* **1999**, *5*, 2464.
[12] J. M. Lehn, *Supramolecular Chemistry – Concepts and Perspectives*, VCH, Weinheim, **1995**.
[13] M. D. Ward, *Chem. Soc. Rev.* **1995**, *24*, 121.
[14] E. C. Constable, J. M. Holmes, *J. Organomet. Chem.* **1986**, *301*, 203.
[15] a) J. P. Collin, M. Beley, J. P. Sauvage, F. Barigeletti, *Inorg. Chim. Acta* **1991**, *186*, 91; b) S. Chodorowski-Kimmes, M. Beley, J. P. Collin, J. P. Sauvage, *Tetrahedron Lett.* **1996**, *37*, 2963; c) F. Barigelletti, B. Ventura, J. P. Collin, R. Kayhanian, P. Gavina, J. P. Sauvage, *Eur. J. Inorg. Chem.* **2000**, 113.
[16] P. Reveco, R. H. Schmehl, W. R. Cherry, F. R. Fronczek, J. Selbin, *Inorg. Chem.* **1985**, *24*, 4078.
[17] A. J. Lees, *Chem. Rev.* **1987**, *87*, 711.
[18] S. Fraysse, C. Coudret, J. P. Launay, *J. Am. Chem. Soc.* **2003**, *125*, 5880.
[19] I. Sasaki, L. Vendier, A. Sournia-Saquet, P. G. Lacroix, *Eur. J. Inorg. Chem.*, DOI: 10.1002/ejic.200600359.
[20] T. L. J. Huang, D. G. Brewer, *Can. J. Chem.* **1981**, *59*, 1689.
[21] M. Heller, U. S. Schubert, *J. Org. Chem.* **2002**, *67*, 8269.
[22] O. Maury, J. P. Guégan, T. Renouard, A. Hilton, P. Dupau, N. Sandon, L. Toupet, H. Le Bozec, *New J. Chem.* **2001**, *25*, 1553.
[23] E. C. Constable, A. M. W. Cargill Thompson, S. Greulich, *J. Chem. Soc., Chem. Commun.* **1993**, 1444.
[24] P. Reveco, J. H. Medley, A. R. Garber, N. S. Bhacca, J. Selbin, *Inorg. Chem.* **1985**, *24*, 1096.
[25] C. Reichardt, E. Harbush-Görnet, *Liebigs Ann. Chem.* **1983**, *5*, 721.
[26] See for example: a) J. P. Costes, J. F. Lamère, C. Lepetit, P. G. Lacroix, F. Dahan, K. Nakatani, *Inorg. Chem.* **2005**, *44*, 1973; b) F. Averseng, P. G. Lacroix, I. Malfant, G. Lenoble, P. Cassoux, K. Nakatani, I. Maltey-Fanton, J. A. Delaire, A. Aukauloo, *Chem. Mater.* **1999**, *11*, 995; c) P. G. Lacroix, S. Di Bella, I. Ledoux, *Chem. Mater.* **1996**, *8*, 541.
[27] G. Olbrechts, R. Strobbe, K. Clays, A. Persoons, *Rev. Sci. Instrum.* **1998**, *69*, 2233.
[28] G. Olbrechts, K. Wostyn, K. Clays, A. Persoons, S. H. Kang, K. Kim, *Chem. Phys. Lett.* **1999**, *308*, 173.
[29] H. T. Uyeda, Y. Zhao, K. Wotsyn, I. Asselbergs, K. Clays, A. Persoons, M. J. Therien, *J. Am. Chem. Soc.* **2002**, *124*, 13806.
[30] G. Sprintschnik, H. W. Sprintschnik, P. P. Kirsch, D. G. Whitten, *J. Am. Chem. Soc.* **1977**, *99*, 4947.
[31] B. Imperiali, T. J. Prins, S. L. Fisher, *J. Org. Chem.* **1993**, *58*, 1613.
[32] J. Uenishi, T. Tanaka, K. Nishiwaki, S. Wakabayashi, S. Oae, H. Tsukube, *J. Org. Chem.* **1993**, *58*, 4382–4388.
[33] N. Walker, D. Stuart, *Acta Crystallogr. Sect. A* **1983**, *39*, 158.
[34] *SIR92 – A program for crystal structure solution*: A. Altomare, G. Cascarano, C. Giacovazzo, A. Guagliardi, *J. Appl. Crystallogr.* **1993**, *26*, 343.
[35] G. M. Sheldrick, *SHELX97 – Programs for Crystal Structure Analysis*, release 97-2, Institut für Anorganische Chemie der Universität, Göttingen, Germany, **1998**.
[36] *WINGX – Integrated System of Windows Programs for the Solution, Refinement and Analysis of Single Crystal X-ray Diffraction Data*, version 1.63: L. J. Farrugia, *J. Appl. Crystallogr.* **1999**, *32*, 837.
[37] *International Tables for X-ray Crystallography*, Kynoch Press, Birmingham, England, **1974**, vol. IV.
[38] *ORTEP3 for Windows*: L. J. Farrugia, *J. Appl. Crystallogr.* **1997**, *30*, 565.
[39] M. J. Frisch, G. W. Trucks, H. B. Schlegel, G. E. Scuseria, M. A. Robb, J. R. Cheeseman, J. A. Montgomery Jr, T. Vreven, K. N. Kudin, J. C. Burant, J. M. Millam, S. S. Iyengar, J. Tomasi, V. Barone, B. Mennucci, M. Cossi, G. Scalmani, N. Rega, G. A. Petersson, H. Nakatsuji, M. Hada, M. Ehara, K. Toyota, R. Fukuda, J. Hasegawa, M. Ishida, T. Nakajima, Y. Honda, O. Kitao, H. Nakai, M. Klene, X. Li, J. E. Knox, H. P. Hratchian, J. B. Cross, C. Adamo, J. Jaramillo, R. Gomperts, R. E. Stratmann, O. Yazyev, A. J. Austin, R. Cammi, C. Pomelli, J. W. Ochterski, P. Y. Ayala, K. Morokuma, G. A. Voth, P. Salvador, J. J. Dannenberg, V. G. Zakrzewski, S. Dapprich, A. D. Daniels, M. C. Strain, O. Farkas, D. K. Malick, A. D. Rabuck, K. Raghavachari, J. B. Foresman, J. V. Ortiz, Q. Cui, A. G. Baboul, S. Clifford, J. Cioslowski, B. B. Stefanov, G. Liu, A. Liashenko, P. Piskorz, I. Komaromi, R. L. Martin, D. J. Fox, T. Keith, M. A. Al-Laham, C. Y. Peng, A. Nanayakkara, M. Challacombe, P. M. W. Gill, B. Johnson, W. Chen, M. W. Wong, C. Gonzalez, J. A. Pople, *Gaussian 03*, revision B.05, Gaussian, Inc., Pittsburgh, PA, **2003**.
[40] a) A. D. Becke, *J. Chem. Phys.* **1993**, *98*, 564; b) C. Lee, W. Yang, R. G. Parr, *Phys. Rev. B* **1988**, *37*, 785.
[41] a) P. J. Hay, W. R. Wadt, *J. Chem. Phys.* **1985**, *82*, 270; b) P. J. Hay, W. R. Wadt, *J. Chem. Phys.* **1985**, *82*, 284; c) P. J. Hay, W. R. Wadt, *J. Chem. Phys.* **1985**, *82*, 299.
[42] D. P. Rillema, D. S. Jones, H. A. Levy, *J. Chem. Soc., Chem. Commun.* **1979**, 849.
[43] M. Muthuraman, R. Masse, J. F. Nicoud, G. R. Desiraju, *Chem. Mater.* **2001**, *13*, 1473.
[44] a) M. C. Zerner, G. Loew, R. Kirchner, U. Mueller-Westerhoff, *J. Am. Chem. Soc.* **1980**, *102*, 589; b) W. P. Anderson, D. Edwards, M. C. Zerner, *Inorg. Chem.* **1986**, *25*, 2728.
[45] *ZINDO*, release 96.0, Molecular Simulations Inc., Cambridge, U. K., **1996**.
[46] a) K. Clays, A. Persoons, *Phys. Rev. Lett.* **1991**, *66*, 2980; b) E. Hendrickx, K. Clays, A. Persoons, *Acc. Chem. Res.* **1998**, *31*, 675.
[47] S. J. Cyvin, J. E. Rauch, J. C. Decius, *J. Chem. Phys.* **1965**, *43*, 4083.
[48] a) J. L. Oudar, J. Chemla, *J. Chem. Phys.* **1977**, *66*, 2664; b) J. L. Oudar, *J. Chem. Phys.* **1977**, *67*, 446.

Received: March 24, 2006
Published Online: July 5, 2006

